ACS Biomaterials SCIENCE & ENGINEERING

Letter

pubs.acs.org/journal/abseba

Membrane Pore Spacing Can Modulate Endothelial Cell–Substrate and Cell–Cell Interactions

Stephanie M. Casillo,[†] Ana P. Peredo,[†] Spencer J. Perry,[†] Henry H. Chung, and Thomas R. Gaborski*

Department of Biomedical Engineering Rochester Institute of Technology, 160 Lomb Memorial Drive, Rochester, New York 14623, United States

Supporting Information

ABSTRACT: Mechanical cues and substrate interaction affect the manner in which cells adhere, spread, migrate and form tissues. With increased interest in tissue-on-a-chip and coculture systems utilizing porous membranes, it is important to understand the role of disrupted surfaces on cellular behavior. Using a transparent glass membrane with defined pore geometries, we investigated endothelial fibronectin fibrillogenesis and formation of focal adhesions as well as development of intercellular junctions. Cells formed fewer focal adhesions and had shorter fibronectin fibrils on porous membranes compared to nonporous controls, which was similar to cell behavior on continuous soft substrates with Young's moduli 7 orders of magnitude lower than glass. Additionally, porous membranes promoted enhanced cell–cell interactions as evidenced by earlier formation of tight junctions. These findings suggest that porous membranes with discontinuous surfaces promote reduced cell–matrix interactions similarly to soft substrates and may enhance tissue and barrier formation.

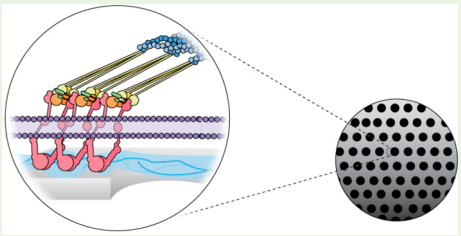

KEYWORDS: *membrane, focal adhesion, fibronectin, substrate stiffness*

There is rapidly growing interest in developing organ-on-a-chip, membrane-supported barrier models, and coculture systems. Porous membranes have been used to support the development of in vitro models of the gut,[1] lung,[2] placenta,[3] blood–brain barrier,[4,5] and other tissues.[6] Additionally, porous membranes are being used to support cell-mediated stem cell differentiation, where a second cell type induces differentiation through physical contact or paracrine signaling.[7,8] Research laboratories are also using porous membranes to support a variety of multicompartment microenvironments that recapitulate complex physiological systems. Advances in these areas are likely to dramatically reduce drug development costs and replace animal models with human cell-based assays.[9]

At the same time, many laboratories are researching more physiologically relevant cell culture substrates and cellular scaffolds.[10] One major area of focus is optimizing substrate stiffness in order to mimic the mechanical properties of tissue.[11,12] There are two commonly used approaches: tunable stiffness hydrogels[13] and engineered deformable microposts.[14] Studies using microposts have typically been designed with varying micropost length to control the effective substrate stiffness felt by the cells. Additionally, deflection of the posts can be used to calculate cellular contractile forces. Hydrogels have also been used to investigate the relationship between traction forces and substrate stiffness by tracking displacement of embedded beads.[15,16] Like microposts, hydrogels of varying stiffness have been shown to affect a variety of cell processes including stem cell differentiation.[17] Although both approaches have been successful in recapitulating physical aspects of tissue, neither directly represents porous membranes used in the burgeoning organ-on-a-chip field. In fact, an array of microposts is the geometric inverse of a porous membrane with respect to cell contact area.

One of the most well studied cell–substrate interactions is the anchoring of cells via focal adhesions (FAs).[18] These interactions are not just important in cellular sensing of the microenvironment during migration, but also in the development and maintenance of barriers such as the vascular wall.[19] Distinct FAs are widely apparent when cells are cultured on stiff surfaces, particularly tissue culture polystyrene (TCPS) and glass.[20] On the other hand, cells growing in three-dimensional tissues and on relatively soft substrates display fewer and smaller FAs.[21] Research on microposts and hydrogels has shown that cellular traction forces are strongly correlated with formation of FAs.[22−24]

Extracellular matrix fibrillogenesis has also been shown to be affected by substrate stiffness.[25] Fibronectin (FN) fibrillogenesis is associated with a cell's ability to generate high traction forces, which in turn requires a relatively stiff supporting matrix or substrate. On the other hand, cells cultured on soft substrates display significantly shorter FN fibrils that appear less organized.[26,27] In fact, the orientation of the fibrils is known to be directed by the cell's actin stress fibers.[25]

In this study, we investigated the effect of membrane pore spacing on cell–substrate interactions and corresponding cell–

Received: January 24, 2017
Accepted: February 16, 2017
Published: February 16, 2017

ACS Publications © XXXX American Chemical Society

DOI: 10.1021/acsbiomaterials.7b00055
ACS Biomater. Sci. Eng. XXXX, XXX, XXX−XXX

cell interactions. We used transparent silicon dioxide (SiO_2; glass) membranes with well-defined micron and submicron pore sizes and spacing that enabled high-resolution imaging of FAs, stress fibers and FN fibrillogenesis. We found that the disrupted surface geometry of these porous membranes negatively affected FA formation and FN fibrillogenesis. While holding total membrane contact area constant, but decreasing pore size and pore spacing, we observed cellular behavior similar to cells cultured on continuous soft substrates.

Use of ultrathin glass SiO_2 membranes enabled visualization of subcellular features and nascent extracellular matrix structures. These membranes were fabricated 300 nm thick with hexagonally patterned 0.5 or 3.0 μm diameter pores (Figure 1). Both porous membranes had approximately 23% porosity and 77% contact area (Figure 1A, B). Fabrication details have been reported previously[28] and can be found in the Supporting Information. Nonporous SiO_2 membranes were fabricated in the same manner and used as control substrates. We chose these pore sizes because of their ability to prevent (0.5 μm) or permit (3.0 μm) cellular migration across the barrier in coculture and leukocyte-endothelial transmigration studies. It is challenging to culture confluent monolayers on membranes with pore sizes >3 μm due to the tendency for endothelial and epithelial transmigration. While polymeric track-etched (TE) membranes with similar pore sizes are widely available, TE membranes have varying pore densities and interpore spacing (Figure 1C, D) that likely affects cell–substrate interactions. We chose to use patterned SiO_2 membranes for controlled pore spacing and excellent imaging properties.

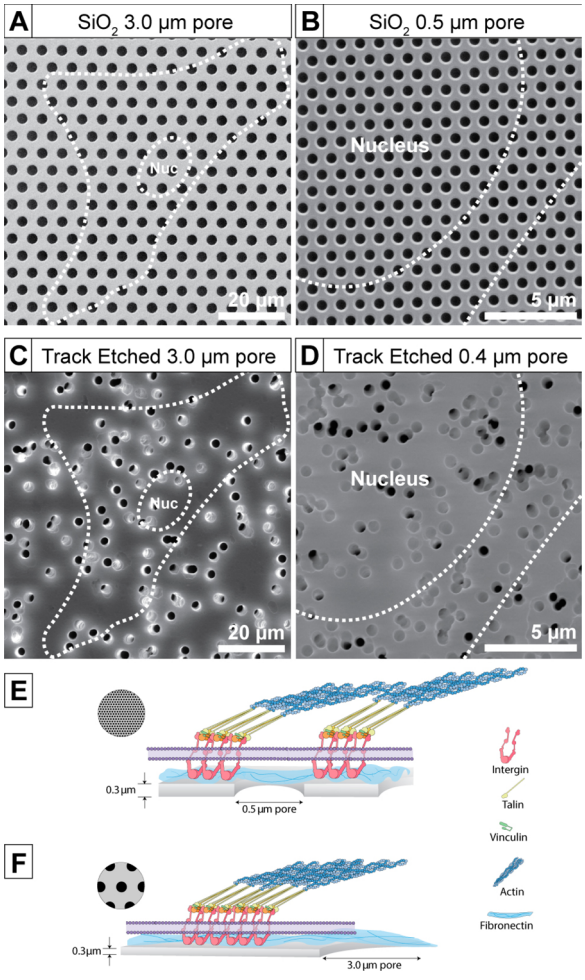

Figure 1. Scanning electron microscopy (SEM) images of 300 nm thick SiO_2 membranes with (A) 3.0 μm and (B) 0.5 μm diameter pores; Greiner Bio-One Thincert track etched high-porosity membranes with (C) 3.0 μm and (D) 0.4 μm diameter pores. Dotted white outline shows the size of a typical cell and its nucleus. (E, F) Illustrations showing potential focal adhesion formations on 0.5 and 3.0 μm diameter pore SiO_2 membranes.

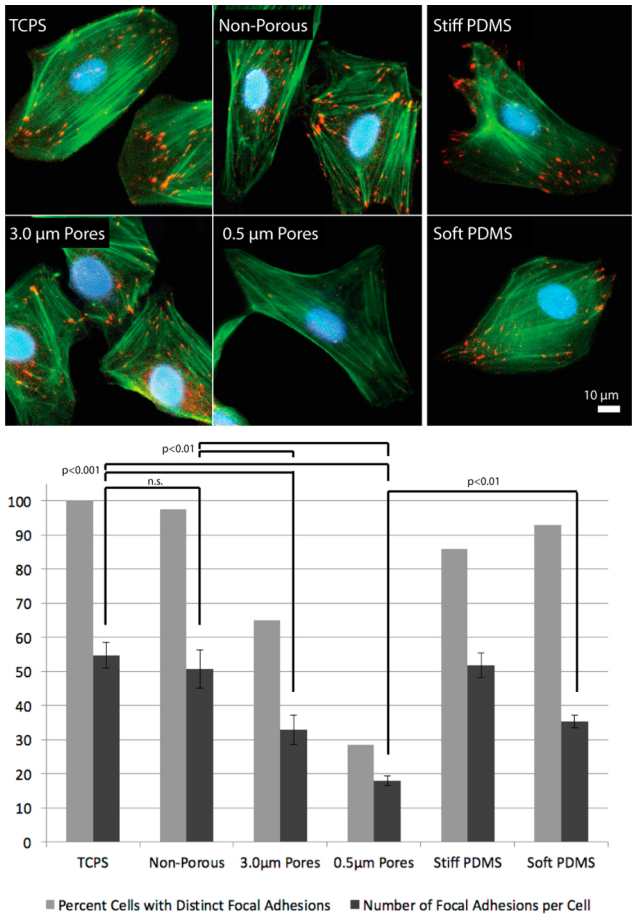

Figure 2. Representative images of endothelial focal adhesions after 24 h on TCPS, SiO_2 membranes, Stiff (2 MPa) PDMS and Soft (5 kPA) PDMS substrates. Cells were stained for nuclei (DAPI, blue), F-actin (phalloidin, green), and focal adhesions (antivinculin, red). Bottom: Quantification of focal adhesion formation after 24 h of culture. Formation of distinct focal adhesions was quantified for all substrates - percent of cells with distinct focal adhesions and number of focal adhesions per cell (n > 20 for each substrate; mean ± standard deviation; one-way ANOVA with a Tukey post hoc analysis).

In addition to investigating cellular behavior on stiff porous substrates, we also studied cell–substrate interactions on more compliant polydimethylsiloxane (PDMS). We used common Sylgard 184, which has Young's modulus of 2 MPa as well as softer Sylgard 527, which has a Young's modulus of just 5 kPa.[29] This is 7 orders of magnitude lower than the modulus of SiO_2 thin films[30] and comparable to tissue. For PDMS experiments, we cast silicone substrates that were >500 μm thick to minimize the influence of the underlying TCPS support. Complete cell culture and immunofluorescence methods are available in the Supporting Information.

DOI: 10.1021/acsbiomaterials.7b00055
ACS Biomater. Sci. Eng. XXXX, XXX, XXX−XXX

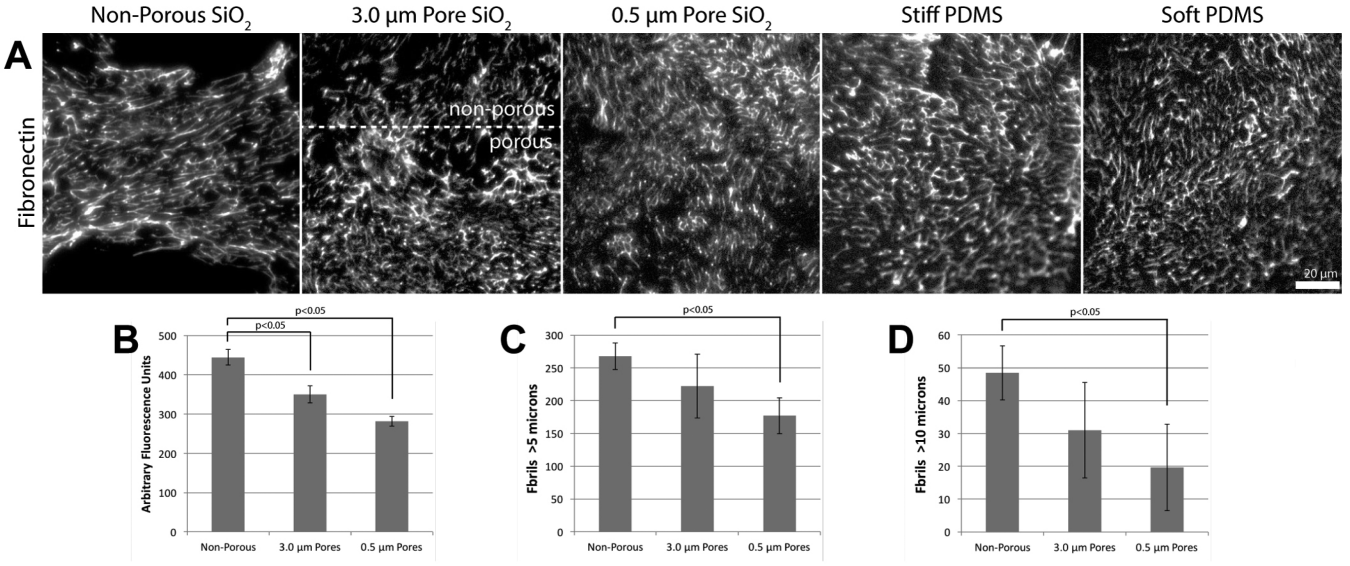

Figure 3. (A) Representative images of endothelial fibronectin fibrillogenesis after 24 h on nonporous, 3.0 and 0.5 μm pore diameter SiO_2 membranes, 2 MPa (Stiff) PDMS and 5 kPa (Soft) PDMS substrates. The image of the 3.0 μm pore diameter SiO_2 membrane shows the boundary between the porous and nonporous regions. (B) Fibronectin density on each SiO_2 membrane substrate was approximated by measuring the mean fluorescence intensity of antifibronectin antibody within 100 × 100 μm regions of interest that were occupied by cells ($n > 15$ for each substrate). (C, D) Fibronectin fibril lengths were also measured using an automated image processing algorithm (comparisons were made using one-way ANOVA with a Tukey post hoc analysis).

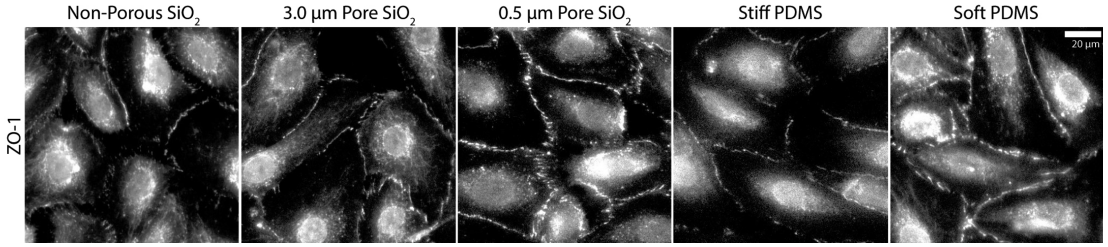

Figure 4. Representative images of tight junction protein ZO-1 after 4 days culture as the cells initially reached confluence on nonporous, 3.0 and 0.5 μm pore diameter SiO_2 membranes, 2 MPa (Stiff) PDMS and 5 kPa (Soft) PDMS substrates. ZO-1 staining was most consistent at cell borders on 0.5 μm pore diameter SiO_2 membranes and soft PDMS.

We investigated the behavior of human umbilical vein endothelial cells (HUVECs) on porous membranes because of their use in vascular barrier models. We suspected that HUVECs may not adhere and spread as well on porous membranes due to the disrupted surface geometry. Cell spread area was measured using image analysis of actin staining after 24 h. There were only minor differences in cell spreading across porous and nonporous substrates (Figure S1). Median spread area on soft PDMS was the lowest. Actin stress fibers were most pronounced on TCPS and nonporous glass membranes, but were visible on all substrates (Figure 2, top). Nearly all cells on TCPS and nonporous glass had distinct FAs with approximately 50 per cell, which is consistent with values in the literature.[31] Similar to previous studies, there were fewer FAs per cell on soft compared to stiff continuous substrates.[32] Two-thirds of cells on 3.0 μm pore membranes displayed FAs. Those cells averaged 33 FAs, significantly fewer than TCPS and nonporous glass. Less than one-third of cells on 0.5 μm pore membranes displayed FAs with an average of just 18 per cell, significantly fewer than even soft PDMS (Figure 2, bottom).

We also investigated FN fibrillogenesis after 24 h. The relationships between substrate stiffness, cellular traction forces and extracellular matrix (ECM) formation has been well studied.[33] Several groups have shown that substrate stiffness is directly related to ECM fibrillogenesis, with endothelial and epithelial cells on stiffer substrates producing longer and more robust FN fibrils.[26,27] This may be due to the greater internal traction forces that can be generated on stiff compared to more compliant substrates, which showed relatively shorter and fewer fibrils. On the other hand, Scott et al. reported that FN assembly by fibroblasts on microposts was roughly constant across multiple stiffnesses.[34] In our experiments, we saw that HUVECs on stiff continuous nonporous SiO_2 membranes produced qualitatively longer and brighter fibrils compared to soft PDMS (Figure 3A). FN fibrils were similar on TCPS and nonporous SiO_2 (Figure S2A). Interestingly, cells on 0.5 μm pore membranes displayed shorter fibrils similar to soft PDMS. We were able to document fibrillogenesis at the border between nonporous and patterned 3.0 μm pores. Fibrils appeared longer over the nonporous region, but significantly shorter over the porous region more than 20 μm from the border confirming the effect of a disrupted surface on FN fibrillogenesis. FN density on SiO_2 substrates was quantified by measuring fluorescence intensity within 100 × 100 μm regions occupied by cells. FN intensity on both porous SiO_2 membranes was significantly less than nonporous SiO_2 (Figure

DOI: 10.1021/acsbiomaterials.7b00055
ACS Biomater. Sci. Eng. XXXX, XXX, XXX−XXX

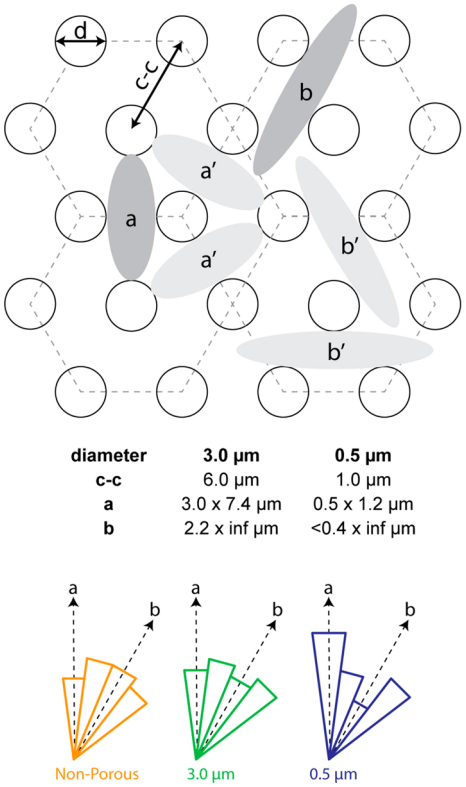

Figure 5. Schematic shows pore spacing and geometries of potential cell−substrate interactions for both 0.5 and 3.0 μm pore size membranes. Due to hexagonal pore spacing, there are three lines of symmetry. Alignment of F-actin stress fibers was measured for nonporous SiO_2, 3.0 and 0.5 μm pore membranes. Normalized radial histograms show the distribution of aligned cells for each substrate (n = 32−37).

3B). The number of FN fibrils greater than 5 and 10 μm in length was also quantified using a custom automated imaging processing algorithm (see Figure S3). Consistent with the qualitative assessment, 0.5 μm pore membranes displayed the fewest long fibrils (Figure 3C, D). Because of the heterogeneity of PDMS background fluorescence, we were unable to quantify FN characteristics on those substrates.

Fewer FAs and less FN fibrillogenesis on porous membranes suggest reduced cell−substrate interactions similar to continuous soft substrates. It was hypothesized by Guo et al.[32] that substrate rigidity regulates the formation of tissues. Specifically, weak cell−substrate interactions may promote cell−cell interactions leading to tissue and barrier formation. To determine if the disrupted surface of a porous membrane would similarly promote cell−cell interactions, we investigated the presence of a tight junctional protein, ZO-1, which regulates barrier formation.[35] We fixed and stained cells at 96 h as they first reached confluence. ZO-1 staining was punctate on nonporous SiO_2 and TCPS (Figure S2B) but robust at cell borders on soft PDMS and 0.5 μm pore membranes (Figure 4). Endothelial monolayers on 3.0 μm pore membranes and stiff PDMS displayed an intermediate degree of ZO-1 staining. These data are consistent with the idea that weak cell−substrate interactions lead to strong cell−cell interactions and earlier barrier formation on porous membranes similarly to soft substrates. After 7 days, ZO-1 labeling did increase on all substrates, suggesting that cell−cell interactions may ultimately dominate for endothelial cells regardless of initial cell−substrate interactions. Although this is consistent with historical success in studying endothelial behavior on continuous and impermeable culture surfaces such as TCPS, discontinuous or porous substrates may promote faster barrier formation. Future studies are necessary to determine if functional barrier properties can be improved or optimized based on reduced cell−substrate interactions.

Data presented thus far suggest that a disrupted surface geometry weakens a cell's interactions with the underlying substrate and leads instead to enhanced cell−cell interactions. Despite identical total contact area on both porous membranes, cells on 0.5 μm pore membranes displayed more pronounced differences in cell−substrate and cell−cell interactions compared to continuous glass and TCPS. This suggests that interpore spacing and limited contact regions are the mechanism behind the differences in behavior. We tested this hypothesis by investigating the alignment of actin stress fibers. Even though very few cells on 0.5 μm pore membranes displayed FAs, it was still possible to measure the alignment of primary stress fibers that terminated at cell−matrix adhesion sites.

The hexagonal spacing of the membrane pores resulted in what we postulated were two regions where the largest cell−substrate interactions could form (Figure 5). We investigated alignment in either the a or b directions as well as the intermediate angles by measuring the angle of the primary actin stress fibers from the a direction (Figure S4). Because the three axes of symmetry, all data was mapped to the primary directions for the radial histogram (Figure 5). Not surprisingly, we found no preferential alignment on the nonporous substrates. Additionally, we found no preference on 3.0 μm pore membranes, suggesting that both a or b contact regions were sufficiently large to support strong cell−substrate interactions. However, cells on 0.5 μm pore membranes had stress fibers that predominately aligned in the a direction, suggesting that contact area confinement due to pore spacing was limiting. Although the b region had theoretically an unlimited length, its width was significantly limited. The a region was shorter, but had greater width and circularity, which may have supported better adhesive interactions.

This data raises the question of whether cells can generate ECM fibrils that span the pores and if this cell-generated matrix can overcome contact area confinement. We stained for vinculin at 6 days and found that cells did indeed form FAs over some pores (Figure S5), indicating that the maturing ECM spanned pores and was sufficiently stable to support cellular traction forces. Interestingly, FAs on 3.0 μm pore membranes at 6 days increased to levels comparable to nonporous substrates. Cellular FAs also increased on 0.5 μm pore membranes, but were still lower than continuous substrates. In contrast, we found no focal adhesions that spanned pores at 24 h on 3.0 μm pore membranes (Figure S4). Because of the submicrometer pore spacing on the 0.5 μm membranes and the limits of conventional optical resolution, it was difficult to definitely state whether or not focal adhesions spanned pores on these smaller pores. The discontinuous nature of the porous membrane in combination with small pore spacing may permanently affect cell−substrate interactions. We believe the close proximity of pores results in many cell−matrix interactions occurring over open pore regions leading to more physiological sensing of ECM stiffness. On the other hand, large pore spacing may facilitate ECM-substrate interactions that result in a far stiffer response when cells

DOI: 10.1021/acsbiomaterials.7b00055
ACS Biomater. Sci. Eng. XXXX, XXX, XXX−XXX

exert traction forces on the matrix. These observations are consistent with the model proposed by Trichet et al. where cellular response to substrate stiffness is large-scale and not due to individual FAs.[12]

In summary, we have shown that the disrupted surface of porous membranes leads to weakened cell−substrate interactions that instead promote cell−cell interactions. This behavior is similar to continuous soft PDMS substrates despite a difference in Young's modulus of over 7 orders of magnitude. Together, these data illustrate that membrane pore properties can be designed to produce a support substrate with an effective stiffness much closer to physiological levels. These results should be extendable to membranes and discontinuous substrates made of a variety of materials. However, these effects are not likely seen to the same degree on track-etched polymeric membranes because of highly variable pore density and greater pore spacing.[36,37]

■ ASSOCIATED CONTENT

Supporting Information

The Supporting Information is available free of charge on the ACS Publications website at DOI: 10.1021/acsbiomaterials.7b00055.

Experimental details on membrane fabrication, cell culture, and image analysis (PDF)

■ AUTHOR INFORMATION

Corresponding Author

*E-mail: trgbme@rit.edu.

ORCID

Thomas R. Gaborski: 0000-0002-3676-3208

Author Contributions

†S.M.C., A.P.P., and S.J.P. contributed equally to this work. The manuscript was written through contributions of all authors. All authors have given approval to the final version of the manuscript.

Funding

Research reported in this publication was supported in part by NIGMS of the National Institutes of Health under award number R35GM119623 to T.G. and the Gleason Family Foundation. The content of this publication is solely the responsibility of the authors and does not necessarily represent the official views of the National Institutes of Health

Notes

The authors declare the following competing financial interest(s): TRG is a co-founder of SiMPore, a nano materials start-up company that commercializes ultrathin membranes.

■ ACKNOWLEDGMENTS

We thank Mehdi Dehghani for taking the scanning electron microscopy membrane images and Joseph Olmsted for creating the cell−substrate interaction illustrations.

■ REFERENCES

(1) Hubatsch, I.; Ragnarsson, E. G. E.; Artursson, P. Determination of drug permeability and prediction of drug absorption in Caco-2 monolayers. *Nat. Protoc.* **2007**, *2* (9), 2111−2119.

(2) Huh, D.; Matthews, B. D.; Mammoto, A.; Montoya-Zavala, M.; Hsin, H. Y.; Ingber, D. E. Reconstituting organ-level lung functions on a chip. *Science* **2010**, *328* (5986), 1662−1668.

(3) Lee, J. S.; Romero, R.; Han, Y. M.; Kim, H. C.; Kim, C. J.; Hong, J.-S.; Huh, D. Placenta-on-a-chip: a novel platform to study the biology of the human placenta. *J. Matern.-Fetal Neonat. Med.* **2016**, *29* (7), 1046−1054.

(4) Ma, S. H.; Lepak, L. A.; Hussain, R. J.; Shain, W.; Shuler, M. L. An endothelial and astrocyte co-culture model of the blood?brain barrier utilizing an ultra-thin, nanofabricated silicon nitride membrane. *Lab Chip* **2005**, *5* (1), 74−85.

(5) Naik, P.; Cucullo, L. In vitro blood−brain barrier models: Current and perspective technologies. *J. Pharm. Sci.* **2012**, *101* (4), 1337−1354.

(6) Huh, D.; Kim, H. J.; Fraser, J. P.; Shea, D. E.; Khan, M.; Bahinski, A.; Hamilton, G. A.; Ingber, D. E. Microfabrication of human organs-on-chips. *Nat. Protoc.* **2013**, *8* (11), 2135−2157.

(7) Mazzocchi, A. R.; Man, A. J.; Desormeaux, J.-P. S.; Gaborski, T. R. Porous Membranes Promote Endothelial Differentiation of Adipose-Derived Stem Cells and Perivascular Interactions. *Cell. Mol. Bioeng.* **2014**, *7* (3), 369−378.

(8) Ryu, S.; Yoo, J.; Jang, Y.; Han, J.; Yu, S. J.; Park, J.; Jung, S. Y.; Ahn, K. H.; Im, S. G.; Char, K.; et al. Nanothin Coculture Membranes with Tunable Pore Architecture and Thermoresponsive Functionality for Transfer-Printable Stem Cell-Derived Cardiac Sheets. *ACS Nano* **2015**, *9* (10), 10186−10202.

(9) Esch, E. W.; Bahinski, A.; Huh, D. Organs-on-chips at the frontiers of drug discovery. *Nat. Rev. Drug Discovery* **2015**, *14* (4), 248−260.

(10) Hickman, G. J.; Boocock, D. J.; Pockley, A. G.; Perry, C. C. The Importance and Clinical Relevance of Surfaces in Tissue Culture. *ACS Biomater. Sci. Eng.* **2016**, *2* (2), 152−164.

(11) Discher, D. E.; Janmey, P.; Wang, Y.-L. Tissue cells feel and respond to the stiffness of their substrate. *Science* **2005**, *310* (5751), 1139−1143.

(12) Trichet, L.; Le Digabel, J.; Hawkins, R. J.; Vedula, S. R. K.; Gupta, M.; Ribrault, C.; Hersen, P.; Voituriez, R.; Ladoux, B. Evidence of a large-scale mechanosensing mechanism for cellular adaptation to substrate stiffness. *Proc. Natl. Acad. Sci. U. S. A.* **2012**, *109* (18), 6933−6938.

(13) Tse, J. R.; Engler, A. J. *Preparation of Hydrogel Substrates with Tunable Mechanical Properties*; John Wiley & Sons: Hoboken, NJ, 2001.

(14) Fu, J.; Wang, Y.-K.; Yang, M. T.; Desai, R. A.; Yu, X.; Liu, Z.; Chen, C. S. Mechanical regulation of cell function with geometrically modulated elastomeric substrates. *Nat. Methods* **2010**, *7* (9), 733−736.

(15) Munevar, S.; Wang, Y.; Dembo, M. Traction force microscopy of migrating normal and H-ras transformed 3T3 fibroblasts. *Biophys. J.* **2001**, *80* (4), 1744−1757.

(16) Califano, J. P.; Reinhart-King, C. A. Substrate Stiffness and Cell Area Predict Cellular Traction Stresses in Single Cells and Cells in Contact. *Cell. Mol. Bioeng.* **2010**, *3* (1), 68−75.

(17) Engler, A. J.; Sen, S.; Sweeney, H. L.; Discher, D. E. Matrix Elasticity Directs Stem Cell Lineage Specification. *Cell* **2006**, *126* (4), 677−689.

(18) Geiger, B.; Spatz, J. P.; Bershadsky, A. D. Environmental sensing through focal adhesions. *Nat. Rev. Mol. Cell Biol.* **2009**, *10* (1), 21−33.

(19) Romer, L. H. Focal Adhesions: Paradigm for a Signaling Nexus. *Circ. Res.* **2006**, *98* (5), 606−616.

(20) Wehrle-Haller, B. Structure and function of focal adhesions. *Curr. Opin. Cell Biol.* **2012**, *24* (1), 116−124.

(21) Harunaga, J. S.; Yamada, K. M. Cell-matrix adhesions in 3D. *Matrix Biol.* **2011**, *30*, 363.

(22) Tan, J. L.; Tien, J.; Pirone, D. M.; Gray, D. S.; Bhadriraju, K.; Chen, C. S. Cells lying on a bed of microneedles: An approach to isolate mechanical force. *Proc. Natl. Acad. Sci. U. S. A.* **2003**, *100* (4), 1484−1489.

(23) Han, S. J.; Bielawski, K. S.; Ting, L. H.; Rodriguez, M. L.; Sniadecki, N. J. Decoupling substrate stiffness, spread area, and micropost density: a close spatial relationship between traction forces and focal adhesions. *Biophys. J.* **2012**, *103*, 640−648.

(24) Beningo, K. A.; Wang, Y.-L. Flexible substrata for the detection of cellular traction forces. *Trends Cell Biol.* **2002**, *12* (2), 79−84.

DOI: 10.1021/acsbiomaterials.7b00055
ACS Biomater. Sci. Eng. XXXX, XXX, XXX−XXX

(25) Lemmon, C. A.; Chen, C. S.; Romer, L. H. Cell Traction Forces Direct Fibronectin Matrix Assembly. *Biophys. J.* **2009**, *96* (2), 729–738.
(26) Palchesko, R. N.; Lathrop, K. L.; Funderburgh, J. L.; Feinberg, A. W. In Vitro Expansion of Corneal Endothelial Cells on Biomimetic Substrates. *Sci. Rep.* **2015**, *5*, 7955.
(27) Eisenberg, J. L.; Safi, A.; Wei, X.; Espinosa, H. D.; Budinger, G. S.; Takawira, D.; Hopkinson, S. B.; Jones, J. C. Substrate stiffness regulates extracellular matrix deposition by alveolar epithelial cells. *Res. Rep. Biol.* **2011**, *2011* (2), 1–12.
(28) Carter, R. N.; Casillo, S. M.; Mazzocchi, A. R.; Desormeaux, J.-P. S.; Roussie, J. A.; Gaborski, T. R. Ultrathin transparent membranes for cellular barrier and co-culture models. *Biofabrication* **2017**, *9* (1), 015019.
(29) Palchesko, R. N.; Zhang, L.; Sun, Y.; Feinberg, A. W. Development of Polydimethylsiloxane Substrates with Tunable Elastic Modulus to Study Cell Mechanobiology in Muscle and Nerve. *PLoS One* **2012**, *7* (12), e51499.
(30) Li, H.; Vlassak, J. J. Determining the elastic modulus and hardness of an ultra-thin film on a substrate using nanoindentation. *J. Mater. Res.* **2009**, *24* (03), 1114–1126.
(31) Kanda, S.; Miyata, Y.; Kanetake, H. Role of focal adhesion formation in migration and morphogenesis of endothelial cells. *Cell. Signalling* **2004**, *16* (11), 1273–1281.
(32) Guo, W.; Frey, M. T.; Burnham, N. A.; Wang, Y. Substrate rigidity regulates the formation and maintenance of tissues. *Biophys. J.* **2006**, *90* (6), 2213–2220.
(33) Singh, P.; Carraher, C.; Schwarzbauer, J. E. Assembly of Fibronectin Extracellular Matrix. *Annu. Rev. Cell Dev. Biol.* **2010**, *26* (1), 397–419.
(34) Scott, L. E.; Mair, D. B.; Narang, J. D.; Feleke, K.; Lemmon, C. A. Fibronectin fibrillogenesis facilitates mechano-dependent cell spreading, force generation, and nuclear size in human embryonic fibroblasts. *Integr Biol. (Camb)* **2015**, *7* (11), 1454–1465.
(35) Tornavaca, O.; Chia, M.; Dufton, N.; Almagro, L. O.; Conway, D. E.; Randi, A. M.; Schwartz, M. A.; Matter, K.; Balda, M. S. ZO-1 controls endothelial adherens junctions, cell–cell tension, angiogenesis, and barrier formation. *J. Cell Biol.* **2015**, *208* (6), 821–838.
(36) Apel, P. Y.; Blonskaya, I. V.; Dmitriev, S. N.; Orelovitch, O.; Sartowska, B. Structure of polycarbonate track-etch membranes: Origin of the "paradoxical" pore shape. *J. Membr. Sci.* **2006**, *282*, 393–400.
(37) Kim, M. Y.; Li, D. J.; Pham, L. K.; Wong, B. G.; Hui, E. E. Microfabrication of high-resolution porous membranes for cell culture. *J. Membr. Sci.* **2014**, *452*, 460–469.

DOI: 10.1021/acsbiomaterials.7b00055
ACS Biomater. Sci. Eng. XXXX, XXX, XXX–XXX

Membrane Pore Spacing Can Modulate Endothelial Cell-Substrate and Cell-Cell Interactions

Stephanie M. Casillo, Ana P. Peredo, Spencer J. Perry, Henry H. Chung and Thomas R. Gaborski

SUPPORTING INFORMATION

Ultrathin Silicon Dioxide (SiO_2) Membrane Fabrication and Device Assembly

SiO_2 membranes were fabricated using conventional microfabrication techniques at the Rochester Institute of Technology Semiconductor Microfabrication Laboratory (SMFL).[1] Briefly, 300 nm of SiO_2 was deposited using plasma enhanced chemical vapor deposition (PECVD) on double-side polished 150 mm diameter wafers. Wafers were backside patterned with a mask that results in 5.4 x 5.4 mm square dies with 2 x 2 mm windows when the wafer was through-etched. The oxide membrane was front-side patterned with an ASML PAS 5500/200 i-line stepper to create 0.5 μm and 3.0 μm pores in a hexagonal tiling pattern with a center-to-center spacing of two diameters (~23% porosity). The pores were patterned and aligned such that there was an approximately 100 micron non-porous exclusion zone at the edge of the suspended membrane. The oxide film was etched with a Drytek 482 Quad Etcher using reactive ion etching. We stabilized the film stress in a slightly tensile state through a 600 °C anneal in nitrogen. This tensile film is substantially more robust than the native film, enabling its use in routine cell culture. The wafer was through-etched from the backside using ethylenediamine pyrocatechol (EDP) in a custom fabricated one-sided heated etch cell as reported previously.[2] After etching, the wafer was cleaved into individual chips. In order to culture cells on the membranes, the chips were bonded to silicone gaskets using a handheld corona surface treatment wand (Nbond, Littleton, CO) as described previously.[3] The silicone gaskets were produced from defined thickness sheets of restricted grade silicone (Silicone Specialty Fabricators, Paso Robles, CA) that was cut using a digital craft cutter.[4] The silicone gaskets were used to help retain cells during seeding.

All substrates were pre-treated for 30 minutes with 1:100 dilution of Geltrex® (0.15 mg/mL concentration) that contains laminin, vitronectin and collagen IV. Substrates were rinsed with PBS immediately prior to seeding cells and were not permitted to air dry. Immunofluorescence confirmed the absence of fibronectin, but a relatively uniform presence of collagen IV on the surface.

Cell Culture

All cell culture and immunofluorescence reagents were purchased from Thermo Fisher (Carlsbad, CA) unless specified otherwise. Pooled HUVECs were cultured in M200 with GIBCO Large Vessel Endothelial Supplement (LVES). Cells were detached and subcultured per manufacturer's instructions using TrypLE. HUVEC media was exchanged every 2-3 days and cells were passaged at 80% confluence. HUVECs were used between passages 3-5.

For focal adhesion and fibronectin experiments, cells were seeded at a density of 800 per membrane. The intent was to achieve 5-10% coverage with minimal cell-cell contact. Cells were cultured for 24 hours, fixed permeabilized and stained as described below. Due to migration of HUVECs over the 24-hour period, fibronectin matrix assembly can appear widespread and suggest a much denser population of cells.

For ZO-1 staining, cells were seeded at 1600 per membrane (10-20% coverage). Cells were fed at 2 days and then fixed and permeabilized at 4 days as they reached confluence. Cells were stained as described below.

Immunofluorescence

Cells were fixed with 3.7% formaldehyde for 15 minutes, washed three times with PBS and then permeabilized with 0.1% Triton X-100 for 3 minutes. Cells were blocked with 1% BSA for 15 minutes and again washed with PBS.

For visualization of stress fibers and focal adhesions, cells were stained with DAPI (300 nM), 1:400 AlexaFluor 488 conjugated phalloidin and 1:100 eFluor570 conjugated anti-vinculin, Clone 7F9 (Affymetrix eBioscience, San Diego, CA).

For visualization of fibronectin fibrillogenesis the cells and substrates were stained with 1:100 AlexaFluor488 conjugated anti-fibronectin, Clone FN-3 (Affymetrix eBioscience, San Diego, CA).

For visualization of tight junctional protein ZO-1 the cells were stained with 1:100 AlexaFluor488 conjugated anti-ZO-1/TJP1, Clone ZO1-1A12 (Affymetrix eBioscience, San Diego, CA).

For visualization of focal adhesions, cells were permeabilized with 0.1% Triton X-100 for 30 seconds, washed twice with PBS, and then fixed with 3.7% formaldehyde for 15 minutes. Cells were blocked with 1% BSA for 15 minutes and again washed with PBS. Cells were stained with DAPI (300nM), 1:400 AlexaFluor 488 conjugated phalloidin, and 1:100 eFluor570 conjugated anti-vinculin Clone 7F9 (Affymetrix eBioscience, San Diego, CA).

Focal adhesions were imaged with 40x and 63x long working distance objectives. Fibronectin and ZO-1 were imaged with a 20x air objective. All imaged were collected on a Leica DMI6000 microscope (Leica Microsystems, Buffalo Grove, IL) using a Rolera em-c^2 camera (QImaging, Surrey, BC Canada).

Distinct focal adhesions were identified as punctate fluorescent (anti-vinculin) features that could be readily identified at 40x using the same exposure time and illumination on all substrates. Focal adhesions were typically elliptical and 2-5 microns in the major axis. Only isolated cells or cells with less than 10% cell-cell contact (as defined by perimeter path) were analyzed for focal adhesions. Total sample size was greater than 20 for each substrate type collected from 3-4 independent membranes or substrates.

Statistical Comparisons

Comparisons between spread area were made using one-way ANOVA with a Tukey post hoc analysis (Figure S1). Comparisons between focal adhesions at 24 hours were made using one-way ANOVA with a Tukey post hoc analysis in Minitab (Figure 2). Percent of cells with distinct focal adhesions is from the sum total across the 3-4 independent membranes or substrates of each type ($n > 20$). Normalized radial histograms of stress fiber alignment (Figure 5) show the distribution of aligned cells ($n = 32$-37 for each substrate from 3-4 independent substrates for each type). Student's unpaired t-test comparisons were made between 1-day and 6-day focal adhesion measurements on non-porous, 0.5 μm and 3.0 μm pore glass membranes (Figure S2). Statistical comparisons of fibronectin intensity (Figure 3 B) and fibril length (Figure 3 C and D) from the different substrate types were each performed *via* one-way ANOVA with a Tukey post hoc analysis ($\alpha = 0.05$).

Cell Spread Area

For cell spreading experiments, HUVEC were seeded at a density of 500 cells/membrane, which was found to minimize the degree of cell-cell contact after 24 hours. After 1, 4, or 24 hours, cells were fixed, permabilized, and stained for nuclei and F-actin cytoskeleton. Four 10x tiled images covering each 2 x 2 mm membrane were analyzed, overlapping regions were excluded. The borders of the cells were identified by thresholding the F-actin cytoskeleton images and then converting to a binary image. The spread-area of each cell was found using the measure tool on each binary object. The DAPI channel was used to confirm that each binary object had a single nucleus and that the cell was not undergoing mitosis. More than 50 cells were analyzed for each substrate type. Box and Whisker plots were created in Microsoft Excel (Seattle, WA) using a custom script. The box represents Q1-Q3 with the median identified as a line. The Whiskers represents Q3 + 1.5 IQR and Q1 – 1.5 IQR. No significant differences were found using one-way ANOVA with a Tukey post hoc analysis.

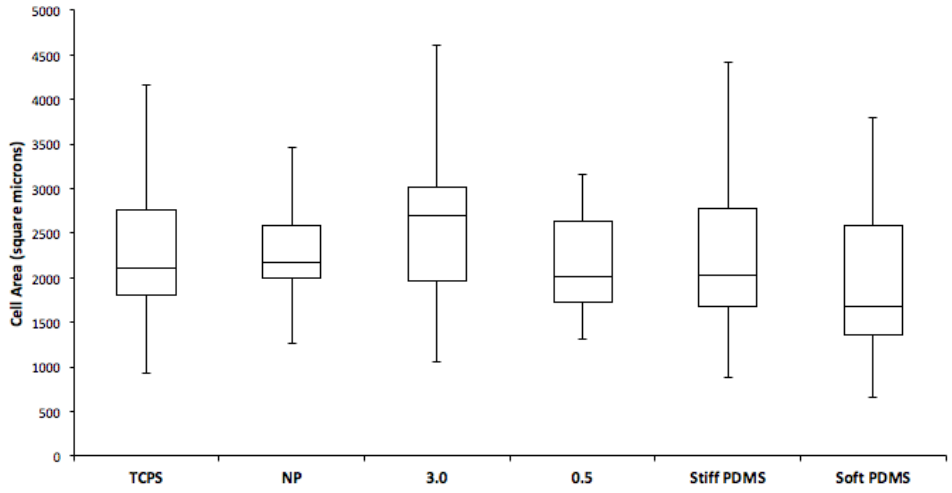

Figure S1. Cell-spread area tissue culture treated polystyrene (TCPS), non-porous, 3.0 μm and 0.5 μm pore diameter SiO_2 membranes after 24 hours. The box plots represent median and IQR of spread area (whiskers are the highest and lowest datum within +/- 1.5 IQR).

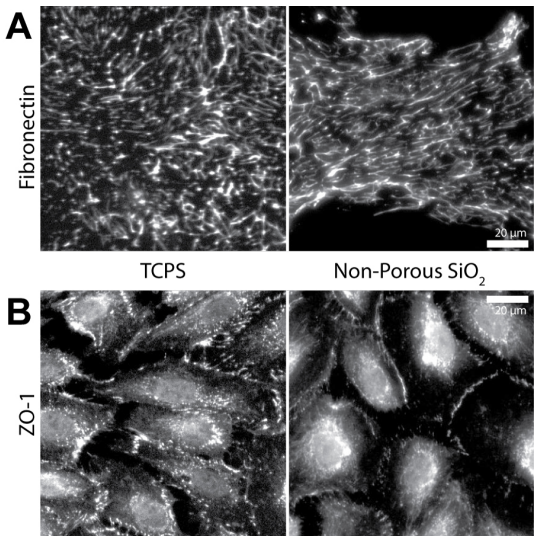

Figure S2. Fluorescent images of Fibronectin and ZO-1 on TCPS and non-porous SiO_2 membranes are similar in morphology and intensity.

Fibronectin Intensity Analysis

For each 10x image of fibronectin fibrils, five 100 µm x 100 µm regions were randomly selected from cellular regions and a 50 µm x 50 µm region was arbitrarily chosen from the non-cellular regions as background. The average intensity of each selected region was background subtracted and pooled together to produce a sample size of at least fifteen for each substrate type collected from multiple (3 or 4) independent substrates. Statistical comparisons of the fibronectin intensities from the different substrate types were performed *via* one-way ANOVA with a Tukey post hoc analysis ($\alpha = 0.05$).

Fibronectin Fibril Length Analysis

For each 40x image of fibronectin fibrils, the edges of the fibronectin fibers were detected using the Laplacian of Gaussian method in MATLAB. Described briefly, the 2nd spatial derivative of image intensity was calculated and the edge was defined at wherever there is a zero-crossing. The half perimeter of the edge was used as the approximation of fiber length. We quantified the total number of long fibers (≥ 5 µm and ≥ 10 µm) across multiple samples (n = 3-4) for each substrate. The numbers of long fibers from the different substrate types were compared *via* one-way ANOVA with a Tukey post hoc analysis ($\alpha = 0.05$).

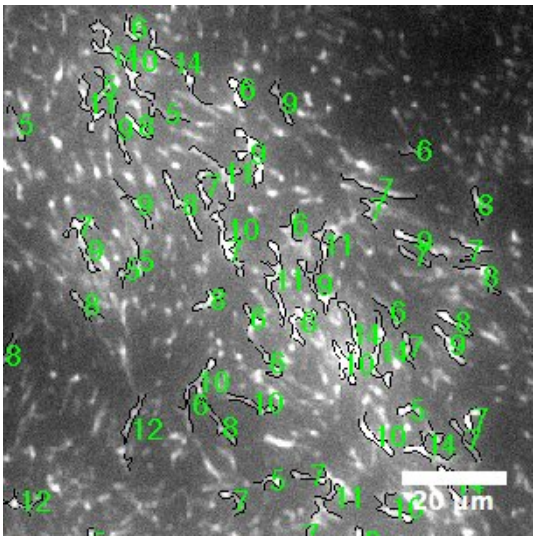

Figure S3. Example of fibronectin fibril length analysis using the Laplacian of Gaussian method on a non-porous SiO_2 membrane. Numbers are the estimated lengths of each detected fibril ≥ 5 µm.

Cell Alignment Analysis

We measured the orientation of a cell's primary actin stress fibers in ImageJ (Figure S5) and categorized the cell as aligned in either ***a*** (-7.5° to 7.5°), between ***a*** and ***b*** (7.5° to 22.5°), ***b*** (22.5° to 37.5°) or between ***b*** and ***a*** (37.5° to 52.5°). All porous membrane images were oriented with the ***a*** direction as shown in Figure S5. Non-porous images were not rotated and should represent a random distribution result. Due to the three axes of symmetry, all angle data was mapped to the primary directions listed above. The sum total within each direction was used to create the radial histograms in Figure 5.

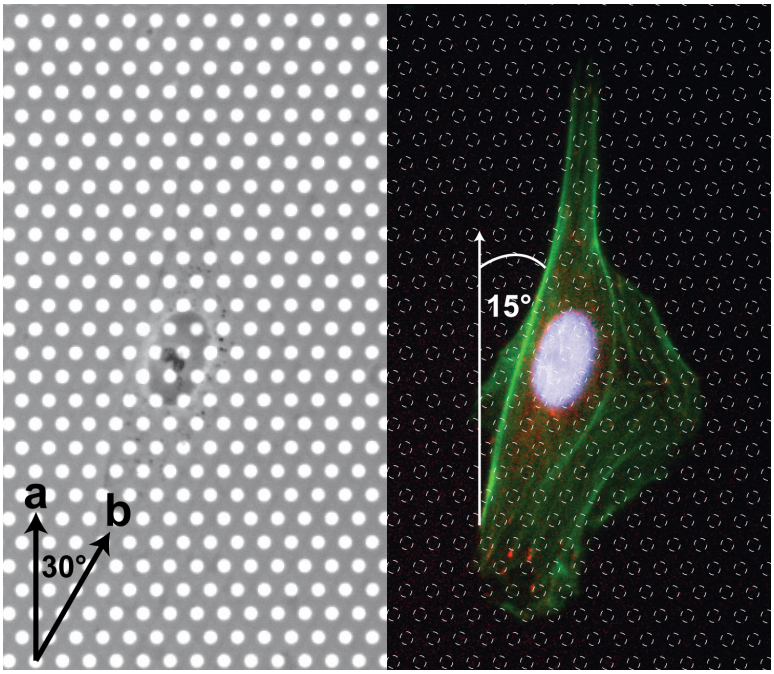

Figure S4. Phase contrast and fluorescence microscopy images of a cell on a SiO_2 show how alignment of F-actin was measured. This representative image also shows that punctate focal adhesions do not significantly overlap pores at 24 hours.

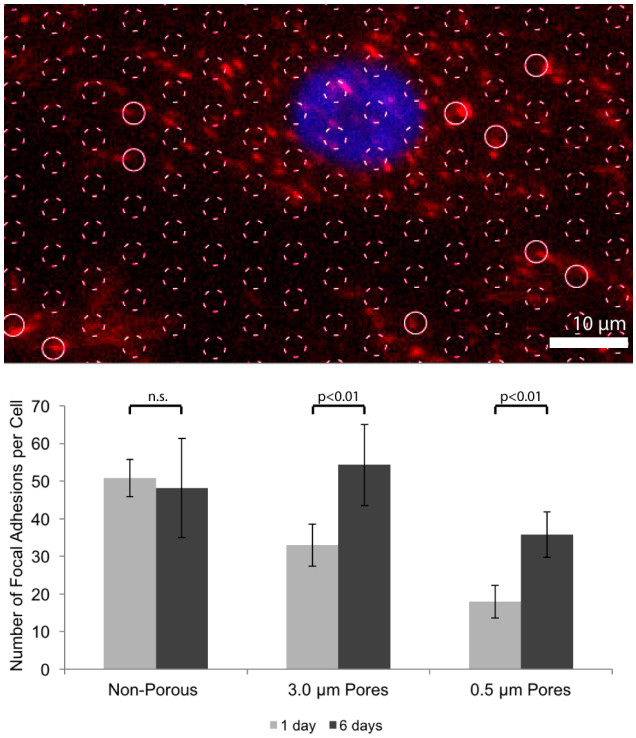

Figure S5. Fluorescent image of a cell on a 3.0 µm pore diameter SiO_2 membrane after 6 days stained for focal adhesions (anti-vinculin, red) and the nucleus (DAPI, blue). White outlines identify locations of a pore. Solid circles indicate where focal adhesions overlap pores. Bottom: Quantification of the number of focal adhesions after 1 day and 6 days ($n > 20$ for each substrate; mean ± standard deviation; Student's unpaired t-test comparisons).

References

(1) Carter, R. N.; Casillo, S. M.; Mazzocchi, A. R.; Desormeaux, J.-P. S.; Roussie, J. A.; Gaborski, T. R. Ultrathin transparent membranes for cellular barrier and co-culture models. Biofabrication 2017, 9 (1), 015019 DOI: 10.1088/1758-5090/aa5ba7.

(2) Striemer, C. C.; Gaborski, T. R.; McGrath, J. L.; Fauchet, P. M. Charge- and size-based separation of macromolecules using ultrathin silicon membranes. Nature 2007, 445 (7129), 749–753 DOI: 10.1038/nature05532.

(3) Yang, C.; Wang, W.; Li, Z. Optimization of corona-triggered PDMS-PDMS bonding method; 2009; pp 319–322.

(4) Yuen, P. K.; Goral, V. N. Low-cost rapid prototyping of flexible microfluidic devices using a desktop digital craft cutter. Lab Chip 2010, 10 (3), 384–387 DOI: 10.1039/b918089c.